DOI: 10.1002/ aelm.201800593

Article type: Full Paper

Substrate-Wide Confined Shear Alignment of Carbon Nanotubes for Thin Film Transistors

*Katherine R. Jinkins, Jason Chan, Robert M. Jacobberger, Arganthaël Berson, and Michael S. Arnold**

K. R. Jinkins, Dr. R. M. Jacobberger, Prof. M. S. Arnold

University of Wisconsin-Madison, Department of Materials Science & Engineering

1509 University Ave., Madison, WI 53706

Email: michael.arnold@wisc.edu

J. Chan, Prof. A. Berson

University of Wisconsin-Madison, Department of Mechanical Engineering

1513 University Ave., Madison, WI 53706

Keywords: aligned, semiconducting, electronics, field effect transistors, large-area

To exploit their exceptional charge transport properties in transistors, semiconducting carbon nanotubes must be assembled onto substrates in aligned arrays comprised of individualized nanotubes at optimal packing densities. However, achieving this control on the wafer-scale is challenging. Here, we investigate solution-based shear in substrate-wide, confined channels to deposit continuous films of

well-aligned, individualized, semiconducting nanotubes. Polymer-wrapped nanotubes in organic ink are forced through sub-mm tall channels, generating shear up to 10,000 s^{-1} uniformly aligning nanotubes across substrates. The ink volume and concentration, channel height, and shear rate dependencies are elucidated. Optimized conditions enable alignment within a ±32° window, at 50 nanotubes μm^{-1}, on 10 × 10 cm^2 substrates. Transistors (channel length of 1 – 5 µm) are fabricated parallel and perpendicular to the alignment. The parallel transistors perform with 7× faster charge carrier mobility (101 and 49 $cm^2V^{-1}s^{-1}$ assuming array and parallel-plate capacitance, respectively) with high on/off ratio of 10^5. The spatial uniformity varies ±10% in density, ±2° in alignment, and ±7% in mobility. Deposition occurs within seconds per wafer, and further substrate scaling is viable. Compared to random networks, aligned nanotube films promise to be a superior platform for applications including sensors, flexible/stretchable electronics, and light emitting and harvesting devices.

1. Introduction

Semiconducting single-walled carbon nanotubes are widely regarded as a promising candidate for next-generation thin film transistors because of their exceptional charge transport properties,[1–4] solution-processability, mechanical resilience,[5] and air-stability. In order to fully exploit nanotubes' fast and directional charge transport properties in thin film transistors, films of highly aligned, individualized, electronics-grade semiconducting nanotubes are needed. These nanotubes must be uniformly deposited over large-area substrates at an intermediate linear packing density of 50 – 200 nanotubes μm^{-1}.[6,7] Alignment is important, as it decreases the number of resistive nanotube-nanotube junctions in the charge percolation pathway, thereby enabling high transistor drive current and mobility.[8,9] Moreover, nanotube individualization and control over packing density are important because the bundling and the formation of multilayers of tubes at high packing densities can result in transistors with low on/off conduction modulation ratio due to electrostatic screening.[10,11] Bundles and multilayers can also decrease on-current due to difficulties in forming low-resistance electrical contacts to tightly spaced nanotubes.[12] On the other hand, if the density of nanotubes is too low, then there are an insufficient number of charge conducting pathways, resulting in poor on-current and mobility. Individualization is also imperative in

applications such as sensors, in which the nanotube surface area must be maximized to increase the number of accessible sites for analyte binding.[13]

Driving nanotube alignment has been difficult, by itself, but concurrently realizing control over packing density, nanotube individualization, uniformity, and large-area scaling has been especially challenging. Most conventional approaches for depositing nanotubes onto substrates (e.g., spin-,[14] blade-[15] and drop-casting;[16] spraying;[17,18] and vacuum filtration[19,20]) yield films of nanotubes that are randomly oriented. Strategies for aligning nanotubes have been pursued; however, many of these approaches have been developed without thin film transistors in mind. For example, the alignment of multi-walled carbon nanotubes has been demonstrated extensively; yet, multi-walled carbon nanotubes are semimetallic and thus are not suitable for transistors.[21,22] Furthermore, techniques for aligning multi-walled carbon nanotubes are generally difficult to translate to aligning single-walled carbon nanotubes, which are considerably smaller than multi-walled nanotubes. The alignment of nanotubes in polymer matrices has also received substantial attention; but this technique yields bulk composites rather than single layers of tubes on surfaces.[23–25] Likewise, recent work has shown that films of aligned nanotubes can be obtained via vacuum filtration under specific conditions.[26] However, these films consist of many stacked layers of nanotubes. Moreover, alignment of nanotubes via liquid crystal phenomena also typically yields multilayers.[27–29]

Methods have been pursued for the more specialized alignment of nanotubes specifically for thin film electronics applications. These methods include directional chemical vapor deposition,[30–33] Langmuir-Blodgett[34] and Schaefer[35] strategies, floating evaporative self-assembly,[36–38] directed evaporation,[39–41] and elastomeric release,[42] among others. Many of these approaches are promising, and significant progress has been made, for example, in producing transistors with high

conductance,[43] with high mobility,[37] or that have aggressively downscaled channel lengths.[44,45] While these methods are promising, more work is needed to refine or identify strategies that are scalable and achieve uniform alignment, individualization, and control over packing density.

Here, solution-based shear is investigated as a means for depositing continuous films of well-aligned, individualized, electronics-grade semiconducting nanotubes onto substrates at the intermediate packing density needed for thin film transistors. Whereas microfluidic channels have been previously utilized to shear-align nanowires[46,47] and nanotubes[48,49] in solution over small areas, here, a substrate-wide deposition strategy is explored for depositing nanotubes to form a uniform, continuous film. For example, we demonstrate uniform deposition on a 10 × 10 cm^2 substrate. Elements of shear have been utilized in other nanotube and nanowire alignment approaches in the past, including blown-bubble assembly,[50] spinning Langmuir method,[51] air-driven directional evaporation,[39–41] and bulk polymer flow.[24] However, additional effort is still required to realize large-area and uniform nanotube films with the attributes (e.g., alignment, individualization, controlled packing density, semiconducting-purity) that are needed to fully exploit nanotubes in electronics.

In general, flow-induced shear is a promising approach for aligning elongated nanostructures. Velocity gradients in a flow field induce a shear force that acts to rotate elongated nanostructures so that their long-axis points in the direction of flow – provided that the magnitude of the velocity gradient exceeds the rotational diffusion coefficient, D_r, of the nanostructure.[52] Smaller nanostructures have larger D_r, and thus, in comparison to larger nanostructures such as nanowires and multi-walled nanotubes, single-walled carbon nanotubes are particularly difficult to align via shear. For example, the D_r of a typical single-walled nanotube (diameter, d, = 1.4 nm;

length, *L,* = 0.5 µm) is ~ 310 s^{-1}, which is 100× larger than the D_r of ~ 3 s^{-1} for a conventional inorganic nanowire (diameter, *d*, = 25 nm; length, *L*, = 2 µm).[46]

Besides their larger D_r, another complication with depositing aligned single-walled nanotubes is maintaining their individualization. Surfactants and polymer wrappers non-covalently bind to nanotubes and are commonly used to individually disperse nanotubes into solvents. These wrappers, however, can inhibit the deposition and "sticking" of nanotubes to target substrates. Furthermore, if these species are only weakly bound to the nanotubes, the nanotubes can problematically coalesce into bundles during deposition. Residues of these surfactants and polymer wrappers can also contaminate the nanotube/electrode and nanotube/nanotube interfaces of thin film transistors, decreasing performance.[43]

2. Results and Discussion

In this work, conjugated polymer wrapped nanotubes dispersed in chloroform are used as a nanotube ink. To create the ink, semiconducting nanotubes are extracted from heterogeneous as-produced powder of nanotubes grown by the arc discharge method using the selective polymer wrapper, poly[(9,9-dioctylfluorenyl-2,7-diyl)-*alt*-*co*-(6,6'-{2,2'-bipyridine})] (PFO-BPy).[38,53] After wrapping, unselected and/or undispersed metallic and semiconducting nanotubes are precipitated from solution via centrifugation. Excess, unbound polymer is then removed from the ink. This procedure yields inks that are well-suited for shear alignment and for thin film transistors.

One advantage of using polymer wrapped nanotubes versus small molecule surfactant encapsulated nanotubes is that in the former case it is possible to remove the excess polymer from free solution while still maintaining a stable suspension of individualized carbon nanotubes. Excess

surfactant or polymer can inhibit the adhesion of carbon nanotubes to the substrate surface, so the removal of excess dispersant is important. Another advantage of using polymer wrapped nanotubes is that the polymer wrapper prevents the carbon nanotubes from forming tightly bound bundles on the substrate surface, which are undesirable in FETs. Finally, conjugated polymers such as PFO-BPy are capable of reducing the relative abundance of metallic nanotubes to less than 0.01%, thereby enabling the fabrication of ultrahigh purity semiconducting nanotube films largely free of problematically metallic nanotube species.[37,43] The extraction process and the preparation of substrates are discussed in more detail in the Experimental section.

The experimental apparatus used for the substrate-wide shear alignment is shown in **Figure 1**. The setup consists of two stainless steel plates (each 6.35 mm thick), a bottom plate on which the substrate is placed, and a top plate with a tube fitting as an input for the semiconducting nanotube ink. The inside of the top plate is polished to a roughness of 23 ± 4 nm (measured via a Zygo interferometer). A channel mask is created to confine the flow of ink and direct it uniformly across the surface of the substrate. The mask is cut from 25.4 to 127 µm thick perfluoroalkoxy (PFA) sheet. Stainless steel spacers are placed outside the channel to act as “hard-stops” that coarsely define the channel height when the PFA is compressed to the spacers. After tightening, bolts along the outside of the plates fasten the top plate to the bottom plate and create a sealed channel. After assembly of the apparatus, the channel height is measured.

The ink is injected and forced through the substrate-wide channel using a syringe pump (Chemyx Nexus 3000), immediately followed by chloroform to “wash” any remaining nanotubes out of the channel. The channel is subsequently rinsed with isopropyl alcohol (IPA) and dried with N_2.

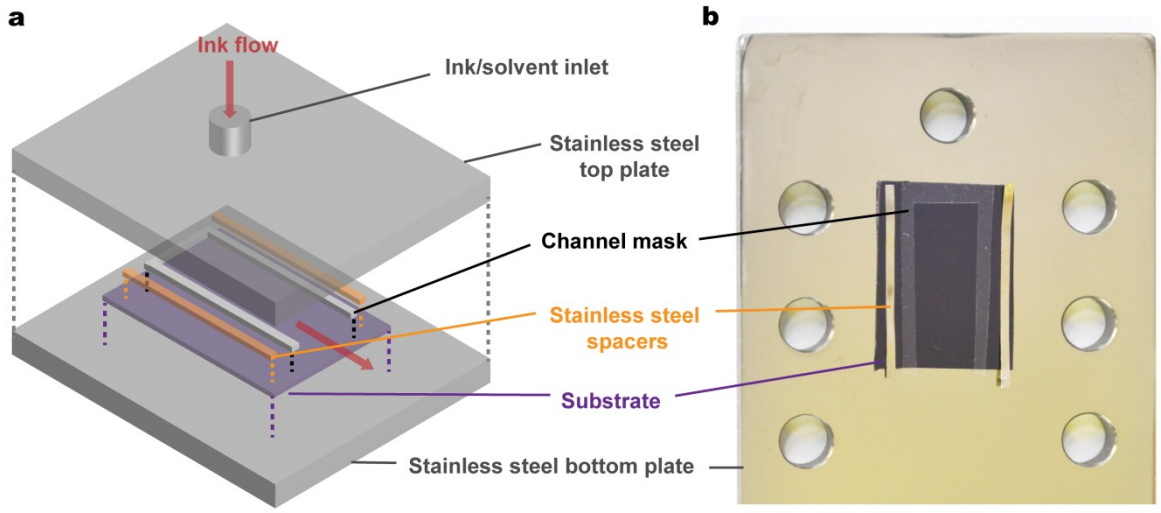

Figure 1. (a) Expanded view schematic and (b) top-view photograph of the experimental wafer-wide confined shear alignment setup with the top plate removed. The setup in the photograph accommodates 2.5 cm wide substrates. The substrate is placed on the stainless steel bottom plate. A channel mask made out of perfluoroalkoxy (PFA) is situated on the substrate to define the area for the ink to flow. The top plate has a tubing inlet to allow ink and solvent to flow across the substrate. Four bolts (M6 × 0.75) with 1.7 N-m of torque are used directly around the substrate to attach the top plate to the bottom plate and seal the channel. The remaining three bolts are hand-tightened. After tightening, the PFA mask compresses until the top plate hits the stainless steel spacers outside the channel mask.

2.1. Effect of Shear Rate on Nanotube Alignment

First, we study the effect of the shear rate on the alignment of the nanotubes. The shear rate during deposition is controlled using two methods: 1) the volumetric flow rate of the ink is varied while all physical dimensions of the channel are constant and 2) the channel height is varied while the volumetric flow rate of ink is constant. The shear rates are calculated assuming a planar Poiseuille flow with a symmetric parabolic velocity profile (see Supporting Information for discussion of the calculation) using the derived formula for shear rate evaluated at the wall of the channel,

$$\frac{dV}{dy} = \frac{6Q}{d^2w} \quad (1)$$

where Q is the volumetric flow rate, w is the width of the channel, and d is the characteristic length of the rectangular channel cross-section. Equation 1 shows that the shear rate increases with Q and $1/d^2$.

After deposition of nanotubes via confined shear alignment with varying shear rates, the degree of alignment is quantified via polarized Raman spectroscopy. The ratio of the nanotube G-band intensity with laser and analyzer polarizations parallel to the direction of alignment (I_{VV}) and perpendicular to the direction of alignment (I_{HH}) is measured at five different locations across the 1 × 1 cm^2 sample areas and then averaged. We approximate that the orientation of the nanotubes within the films follows a wrapped normal distribution. In this case, the half-width at half-maximum (HWHM) of the distribution can be related to the I_{VV}/I_{HH} ratio. A larger I_{VV}/I_{HH} ratio corresponds to a smaller HWHM, indicating less angular spread and a greater degree of alignment within the nanotube film. An HWHM of 0 and 90° corresponds to absolute unidirectional and random alignment, respectively. The entire process for measuring and calculating the HWHM is outlined in the Supporting Information.

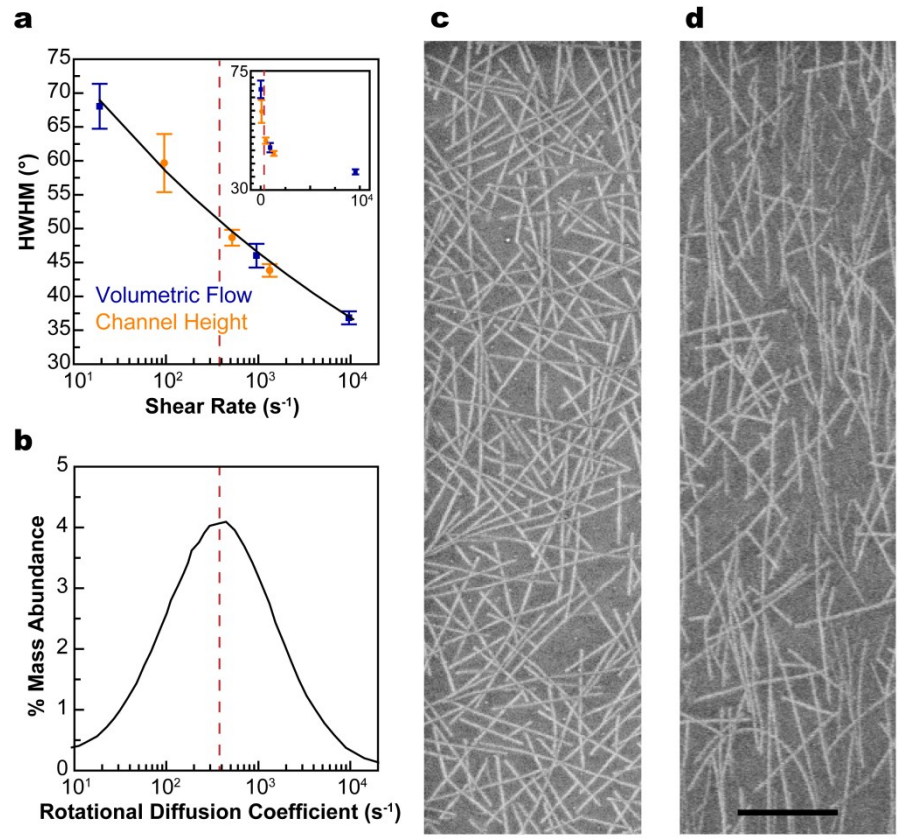

Figure 2. Effect of shear rate on nanotube alignment. (a) Half-width at half-maximum (HWHM) of alignment within a confined shear aligned nanotube film measured via polarized Raman spectroscopy as a function of shear rate plotted on a linear-log scale. Alignment increases with increasing shear rate, following a power-law with an exponent of -0.10, regardless of the method used to adjust shear (blue squares—volumetric flow rate is varied, orange circles—channel height is varied). The inset is the same data plotted on a linear-linear scale. (b) The percent mass abundance of nanotubes with a given rotational diffusion coefficient as calculated from the nanotube length distribution fit from Brady et al.[37] The red dashed line at 386 s^{-1} in both graphs in (a) and in (b) is the rotational diffusion coefficient with the greatest percent abundance in our nanotube inks. (c-d) SEM micrographs of nanotubes deposited on 90 nm of SiO_2 on Si using a shear rate of 19 and 9600 s^{-1}, respectively, from the volumetric flow rate series. The fluid flow direction is top to bottom of the page. Scale bar is 500 nm.

Figure 2a plots the HWHM of the alignment for films fabricated via confined shear alignment at different shear rates (the inset shows the same data plotted on a linear-linear scale). Regardless

of whether the volumetric flow rate or channel height is varied, the alignment of the nanotubes increases with increasing shear rate. For example, the HWHM decreases from 68 to 37° when the shear rate is increased from 19 to 9,600 s^{-1} by increasing the volumetric flow rate from 100 µL min^{-1} to 50 mL min^{-1} at a fixed channel height of 120 µm and channel width of 9.4 mm. The HWHM also decreases from 59 to 43° when the shear rate is increased from 96 to 1330 s^{-1} by decreasing the channel height from 235 µm to 31 µm at a fixed flow rate of 500 µL min^{-1} and channel width of 9.4 mm. The concentration of nanotubes in the ink is 60 µg mL^{-1} for both series, and the ink volume that is flowed through the channel is 285 µL and 170 µL for the volumetric flow and channel height series, respectively.

Alignment is expected when the shear rate is much greater than the rotational diffusion coefficient, D_r.[52] We therefore calculate the distribution of D_r in our nanotube inks (d = 1.5 nm) using the length distribution of our nanotubes and Equation 5 from Tirado et al.,[54]

$$D_r = \frac{3k_BT}{\pi\eta_0 {L_r}^3}\left(\ln\left(\frac{L_r}{d_r}\right) + \delta_\perp\right) \qquad (2)$$

where k_B is the Boltzmann constant, T is the temperature, η_0 is the viscosity, and L_r and d_r are the rod length and diameter, respectively. $\delta_\perp$ is related to the rod length/diameter ratio (L_r/d_r) and encompasses so-called end-effect corrections, discussed in more detail by Tirado et al. This equation assumes that the nanotubes are in an infinitely diluted state (i.e., no interactions with other nanotubes or objects in solution).[54] From this equation, the percent mass abundance of nanotubes with a given D_r is plotted in **Figure 2b**, where the red dashed vertical line in Figures 2a and b corresponds to the rotational diffusion coefficient with the greatest abundance, ~386 s^{-1}. However, this D_r is likely an overestimate, as the presence and interaction of nanotubes with other nanotubes

or free PFO-BPy in solution will, to some extent, reduce the D_r (see Supporting Information for discussion of the calculation).

In bulk solution, the degree of alignment attainable via shear is expected to follow a power-law dependence with an exponent of -0.33.[55,56] In contrast, we observe an exponent of -0.10. This discrepancy is likely in part due to the D_r polydispersity within our nanotube inks (Figure 2b) and also that the polarized Raman measurement itself is nonlinear. This difference in exponent may also indicate that some of the alignment obtained in the bulk of the solution is lost as the nanotubes interact with the substrate as they are deposited. For example, if the front end of a nanotube that is well-aligned in bulk solution adheres to the substrate before the rest of the nanotube can adhere, then this nanotube will rotate about its front end, pushed by the flow, until the trailing end adheres to the substrate. This scenario may give rise to the misaligned 'U' shaped nanotubes that we commonly observe (see, for example, the bottom of **Figure 2d** to the left and above the scale bar or **Figure S5**).

2.2. Effect of Nanotube Ink Concentration and Volume on Confined Shear Alignment

Control over nanotube packing density within aligned nanotube films is vital to optimize the performance of nanotubes for specific applications. We expect that by increasing the number of nanotubes that flow over the substrate, more nanotubes will deposit on the substrate, and it may be possible to control the packing density. We therefore study the effect of ink concentration and ink volume on the packing density. After deposition of nanotube films via confined shear alignment, the packing density is determined from maps of the G-band Raman intensity, as discussed in the Experimental section.

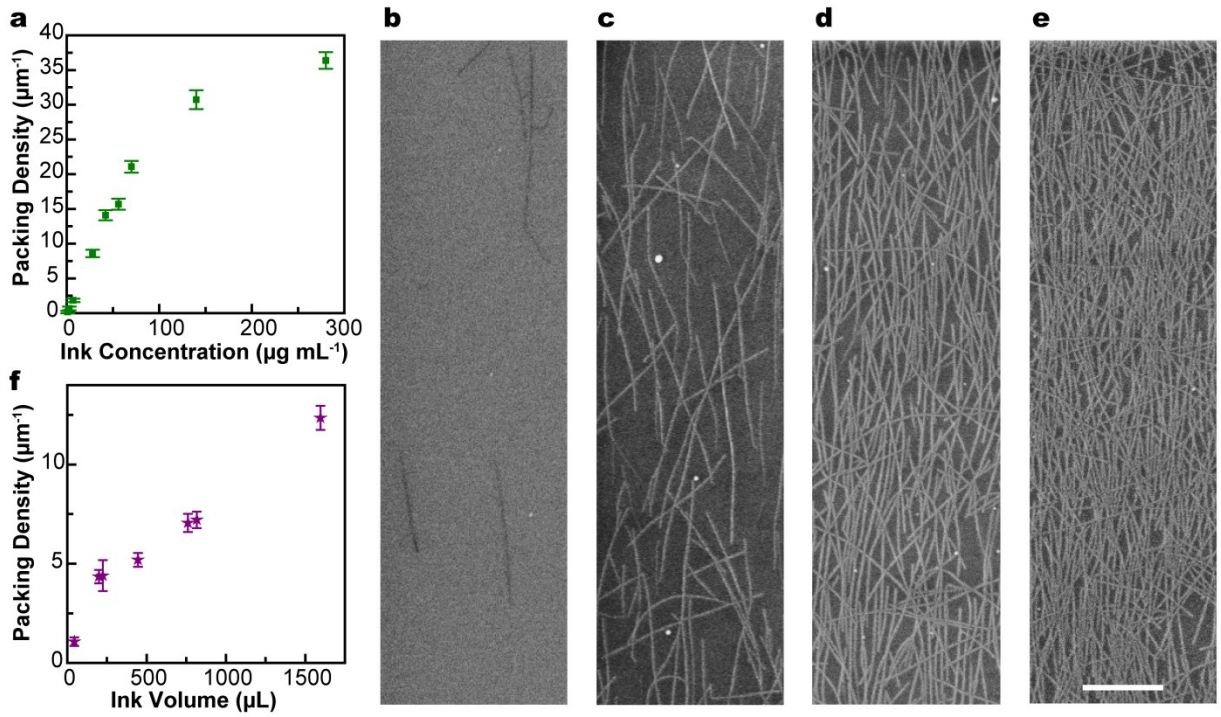

Figure 3. Effect of nanotube ink concentration and ink volume on packing density. (a) Plot of packing density versus ink concentration (at constant ink volume of 250 µL). (b-e) SEM images of four films from part (a) prepared at ink concentrations of 2.8, 42, 140, and 280 µg mL^{-1}, respectively, with resulting packing densities of 0.7, 14, 31, and 36 μm^{-1}, respectively. Scale bar is 500 nm. The fluid flow direction is from top to bottom of the page. In part (a), the packing density increases steeply with increasing ink concentration until a density of ~30 μm^{-1} is reached, and then increases more slowly. Our hypothesis is that the packing density begins to saturate at 30 μm^{-1} because at this density, newly deposited nanotubes must adhere to the substrate by sticking to previously deposited nanotubes as opposed to sticking to the bare substrate. (f) Plot of packing density as a function of nanotube ink volume (at constant ink concentration of 14 µg mL^{-1}). For these data, the channel height is 120 µm, the volumetric flow rate is 100 mL min^{-1}, and the channel width is 9.4 mm.

As shown in **Figure 3**, both the nanotube ink concentration and ink volume can be used to control nanotube packing density in films fabricated via confined shear alignment. The data in **Figure 3a** and SEM micrographs in **Figure 3c-e** illustrate the effect of ink concentration on nanotube packing density at a fixed volume of 250 µL. At low concentrations, the packing density increases steeply

with ink concentration until a packing density of ~30 μm^{-1} is reached. At this point, the rate at which nanotubes deposit decreases, and the packing density increases more slowly with ink concentration. An SEM micrograph of a film deposited at the condition at which the slope transitions from steep to shallow is shown in Figure 3d. At this density of 30 nanotubes μm^{-1}, nanotubes flowing across the substrate cannot adsorb to the bare substrate without overlapping previously deposited nanotubes, slowing the rate at which nanotubes adsorb.

The effect of ink volume on nanotube packing density at constant ink concentration of 14 µg mL^{-1} is also shown in **Figure 3f**. The packing density increases as the volume of ink that is flowed over the substrate increases. An initial steep increase in packing density is observed when the ink volume is increased from 45 to 250 µL. It is unclear what causes the sharp increase in packing density from ~50 to 250 µL, but we hypothesize that it could be due to a secondary effect from the leading ink/air interface or a concentration gradient within the ink that becomes more prevalent at lower ink volumes.

2.3. FETs Fabricated from Confined Shear Aligned Carbon Nanotube Arrays

Charge transport measurements are conducted using a field-effect transistor (FET) architecture to elucidate the effect of alignment and packing density on the mobility of highly pure semiconducting nanotube films deposited via confined shear alignment. These measurements are conducted on aligned films of nanotubes with an HWHM of 40°. After deposition of the nanotubes on 15 nm SiO_2 on Si substrates, isolated regions of nanotubes with width W_{ch} = 10 µm are defined using electron-beam lithography and reactive ion etching. The films are then immersed in boiling toluene to remove excess PFO-BPy and vacuum annealed to partially decompose the PFO-BPy and

remove chlorine impurities introduced on the nanotubes from dispersing in chloroform.[43] This rinsing and vacuum anneal treatment removes the sidechains but not the backbone of the PFO-BPy wrapper. Complete removal of the polymer backbone is possible but has not yet been shown to further improve aligned nanotube FET performance.[57,58] Next, source and drain electrodes with a channel length L_{ch} of 0.5–5 µm are patterned within the isolated regions of nanotubes via electron-beam lithography, development, and thermal deposition of 17.5 nm of Pd and 17.5 nm of Au.

The effect of nanotube alignment on charge transport is studied by aligning the mobility direction of the channels of the FETs to be parallel to the direction of alignment in the nanotube films (termed "parallel FETs", **Figure 4a**) and perpendicular to the direction of alignment in the nanotube films (termed "perpendicular FETs", **Figure 4b**). Roughly four parallel and perpendicular FETs, with nanotube packing density of 59 μm^{-1}, are measured at L_{ch} of 0.5, 1, 2, 3, and 5 µm using a source-drain bias V_{DS} of -1 V.

Representative source-drain current I_{DS} versus gate-source bias V_{GS} curves of parallel and perpendicular FETs with L_{ch} of 1 µm are shown in **Figure 4c** for the forward V_{GS} sweep (negative to positive voltage). Hysteresis is observed in the full sweeps, as shown in **Figure S6**, which is expected for nanotube FETs on SiO_2 substrates and measured in ambient conditions. The mobility of the parallel FETs is 7× higher than that of the perpendicular FETs. For the 59 μm^{-1} packing density devices, the on/off ratio of the parallel FETs is always greater than 2×10^5 and is, on average, 6×10^5, while the on/off ratio of the perpendicular FETs is always higher than 6×10^3 and is, on average, 2.5×10^5. Measurement of the intrinsic off-current of both parallel and perpendicular FETs is prevented by capacitive current from the SiO_2 (I_{GS} versus V_{GS} curves are shown in Figure S6), and therefore the intrinsic on/off ratios are expected to be higher than what is measured here. Regardless, these data

indicate that the high degree of alignment of the nanotube films deposited by confined shear alignment directly results in improvements in both the on-current and on/off ratio of the FETs.

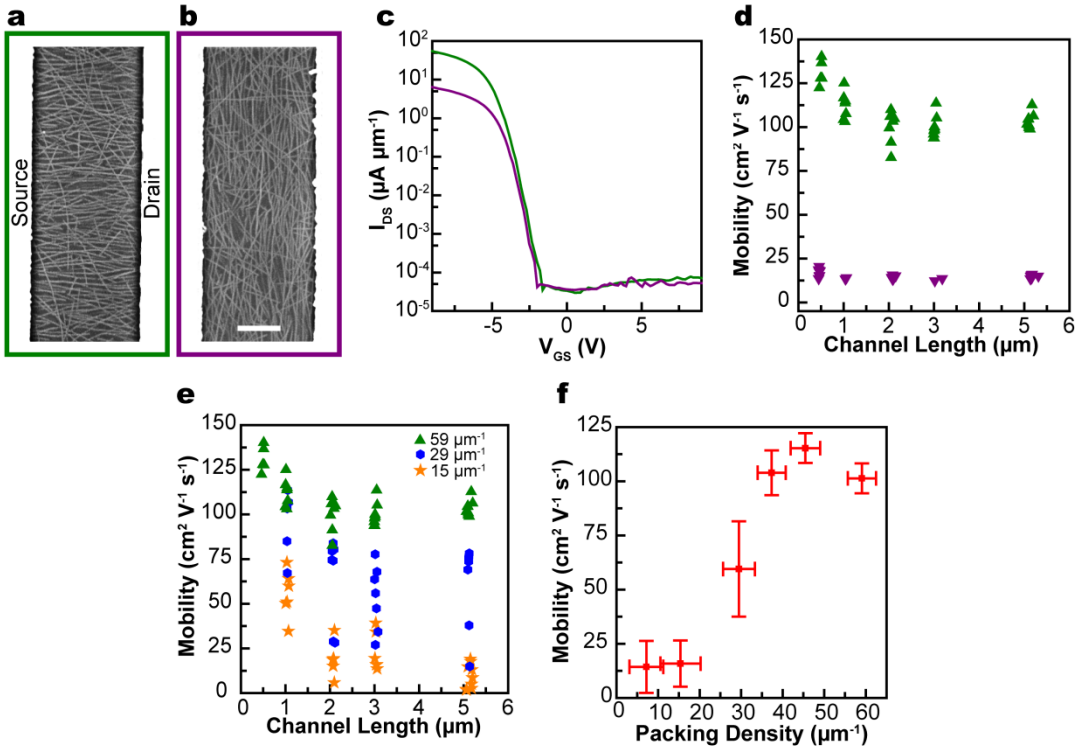

Figure 4. FETs fabricated from confined shear aligned nanotube films. (a-b) SEM micrographs of FETs in which the direction of nanotube alignment is oriented parallel (a) and perpendicular (b) to the channel that is defined by the source and drain electrodes. Scale bar is 500 nm. (c) Representative I_{DS} versus V_{GS} curves measured at V_{DS} of -1 V of the parallel (green) and perpendicular (purple) nanotube FETs with L_{ch} = 1 μm and packing density of 59 μm^{-1}. (d) Extracted hole mobility of parallel (green) and perpendicular (purple) nanotube FETs as a function of L_{ch} using a packing density of 59 μm^{-1}. (e) Extracted hole mobility of parallel FETs as a function of L_{ch} using a packing density of 15 (orange stars), 29 (blue hexagons), and 59 (green triangles) μm^{-1}. (f) Average hole mobility of parallel FETs with L_{ch} = 2 – 5 μm as a function of nanotube packing density. For this data, the PFA mask and channel height are 127 μm and 120 μm, respectively. The ink volume is 250 μL. The volumetric flow rate is 100 mL min^{-1}. The width of nanotube deposition for each film is 10.5 mm. The mobility plotted in parts d-f is calculated using the array capacitance (see main text).

The hole mobility of the nanotube FETs with packing density of 59 μm^{-1} is plotted against L_{ch} for parallel and perpendicular FETs in **Figure 4d**, where the mobility is calculated as

$$\mu = \frac{L_{ch} g_{ch}}{C_{array} W_{ch} V_{DS}} \quad (3)$$

where g_{ch} is the maximum magnitude of the slope of the I_{DS} versus V_{GS} curve (i.e., the transconductance), and C_{array} is the capacitance of the nanotube array and is a function of nanotube packing density. At each L_{ch}, a greater than 7× increase in mobility is observed for parallel FETs compared to perpendicular FETs, indicating that the mobility of these FETs is improved due to the alignment of the confined shear aligned nanotube films. The average mobility of the parallel and perpendicular FETs with L_{ch} of 2 – 5 µm (where the mobility is fairly constant, seen in Figure 4d) is 101 and 14 $cm^2V^{-1}s^{-1}$, respectively, assuming an array capacitance, and 49 and 7 $cm^2V^{-1}s^{-1}$, respectively, assuming a parallel plate capacitance. The array capacitance is calculated from Eq. 3 of Brady et al.[37] and more accurately quantifies the channel-gate capacitance since the separation between nanotubes exceeds the gate dielectric thickness. There is a slight increase in mobility for parallel FETs at L_{ch} less than 1 µm, which is likely due to a larger proportion of the nanotubes directly spanning the source and drain electrodes. In the case where the L_{ch} is greater than 1 µm, nanotubes infrequently directly span the source and drain electrodes and therefore charge must be transferred from tube to tube via a percolating network. It has previously been shown that these tube/tube junctions increase the resistance of the FETs. Consequently, in long channel devices in which L_{ch} is much greater than the average nanotube length, it is important to increase alignment so as to reduce the number of nanotube/nanotube junctions that charges need to traverse in order to cross the channel, thereby reducing the channel resistance and increasing the on-current. If the degree of

alignment is too high, however, the nanotubes will cease to overlap, reducing the number of percolation pathways over which charge can be transported, decreasing the on-current.

In addition to alignment, the packing density of the nanotubes can also affect the performance of nanotube FETs by varying the density of charge percolation pathways. We therefore study the effect of packing density on the mobility of parallel FETs (which show better charge transport than perpendicular FETs) as a function of L_{ch} from 0.5 to 5 µm. **Figure 4e** shows that the mobility increases for all L_{ch} with increasing packing density from 15 to 29 to 59 μm^{-1}. Similar to the parallel FETs in Figure 4d, the mobility slightly increases as the L_{ch} decreases below 1 µm.

The average mobility of parallel FETs with L_{ch} of 2 – 5 µm (the range of L_{ch} over which the mobility is relatively constant in Figure 4d,e) is plotted as a function of packing density in **Figure 4f**. We observe a steep increase in mobility at approximately 30 μm^{-1}. We attribute this increase in mobility to an increase in the number of charge percolation pathways as the packing density is increased. The mobility saturates at a packing density of 45 μm^{-1}, indicating that this is the optimal packing density for confined shear aligned films with an HWHM of 40°. Our FET performance is consistent with other mobility values in literature (0.4 – 287 $cm^2V^{-1}s^{-1}$) reported for aligned carbon nanotube FETs (L_{ch} > 500 nm) fabricated via post-synthetic assembly with on/off ratios greater than 10^3.[28,37,59,60] We expect that FETs with even higher mobility can be achieved with nanotube films deposited via confined shear alignment by further increasing both the degree of alignment, so as to reduce the number of nanotube crossings that charges must traverse from the source to the drain, and the packing density, so as to increase the number of percolation pathways in the channel.

2.4. Aligned nanotube Arrays over 8 × 8 cm^2 via Confined Shear Alignment

It is clear from these data that films of nanotubes with high degree of alignment, controlled packing density, and promising charge transport properties for TFTs can be deposited onto substrates from solution using confined shear alignment. We next explore the ability of confined shear alignment to scale to large areas to deposit uniform films of aligned nanotubes over the wafer scale.

In order to increase the deposition area, we simply increase the size of the confined shear alignment apparatus to accommodate a larger 10 × 10 cm^2 wafer. We also utilize 19.0 mm thick steel sheets for the top and bottom plates to reduce the bowing across the channel. A small trough spanning across the top of the channel is milled around the tube fitting adapter on the inside of the top plate as shown in **Figure S7**. This inset allows the ink to collect first before flowing across the substrate to ensure uniform flow across the relatively large substrate. The inside of the top plate is polished to a roughness of 92 ± 22 nm (measured via Zygo interferometry) to minimize the deviation in channel height, and therefore the shear rate, over the substrate and increase deposition uniformity. In order to deposit nanotubes over a 8 × 8 cm^2 area of the substrate, 2 mL of ink at a concentration of 80 μg mL^{-1} is flowed at a shear rate of 10,700 s^{-1}, which is achieved using a volumetric flow rate of 100 mL min^{-1} and channel height of 30.4 μm. After deposition, the sample is dried using a critical point dryer (Tousimis Automegasamdri 915b) to prevent surface tension during drying to tear or delaminate the nanotube film.

An optical image, obtained using a conventional digital camera (Nikon D3100), of the resulting sample deposited over 8 × 8 cm^2 onto 90 nm of SiO_2 on Si is shown in **Figure 5a**.

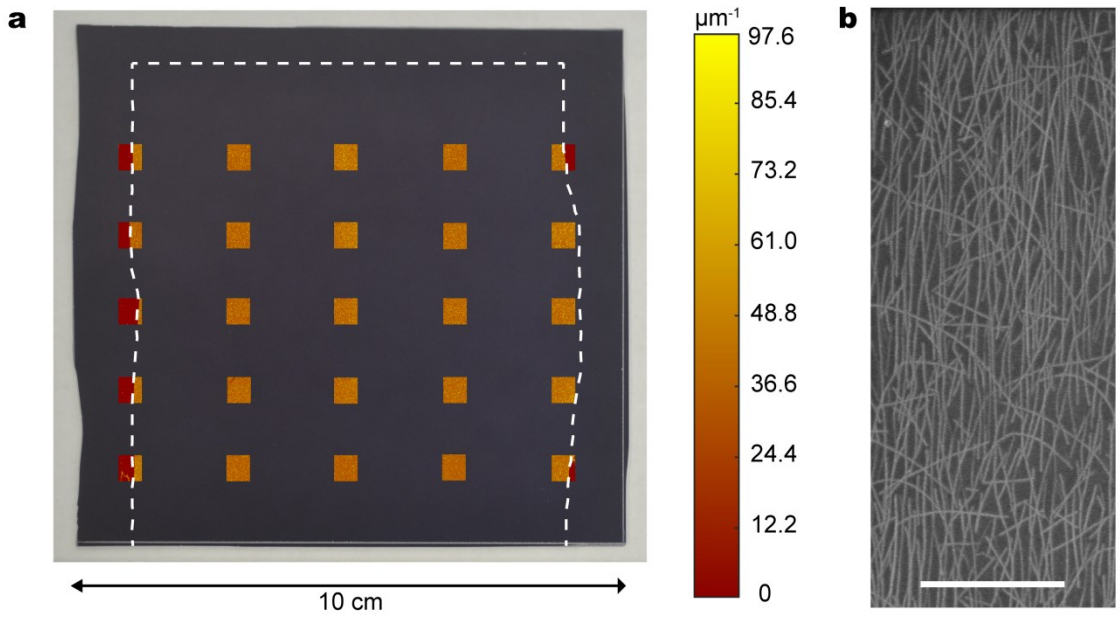

Figure 5. Confined shear aligned nanotube film deposited across an 8 × 8 cm^2 area on 90 nm of SiO_2 on Si. (a) Raman spectroscopy map of the nanotube packing density overlaid on an optical image of the sample. The white dashed line indicates the approximate edges of the mask used to define the deposition channel. (b) SEM micrograph of the aligned nanotubes (light contrast) within the confined shear aligned film shown in (a). Scale bar is 1 μm.

To evaluate film uniformity, smaller Raman spectroscopy maps (each with area of 0.5 × 0.5 cm^2) of the nanotube packing density are measured in a grid across an 8 × 8 cm^2 area. This grid of maps is measured instead of the full area of the sample due to instrument limitations. These smaller Raman maps are shown in Figure 5a overlaid on the photograph. The average packing density across the channel area measured by comparing the average packing density in each map is 48.8 ± 4.8 μm^{-1}. A second grid of 25, smaller Raman maps (250 × 250 μm^2 area) over a similar area (6.8 × 6.0 cm^2) are measured and the packing density is 47.2 ± 5.0 μm^{-1}, indicating high uniformity within the film across multiple length scales. An example Raman map from this grid of 250 × 250 μm^2 maps is shown in

Figure S8. The HWHM alignment within the film measured using polarized Raman spectroscopy across a ~6 × 6 cm^2 area of the nanotube film is 32.3 ± 1.9°. These results demonstrate that the area of deposition in the confined shear alignment method can be easily and simply scaled to achieve aligned nanotube films of nanotubes with relatively uniform packing density over large areas.

3. Conclusion

The alignment of individualized, electronics-grade semiconducting carbon nanotubes in uniform, continuous films at packing densities relevant for electronics has been a challenge for many years. While significant progress has been made toward this goal, no single technique has accomplished all of these objectives. Here, we demonstrate that confined shear alignment is an attractive candidate for achieving these aims.

We show that the nanotube ink concentration and volume can both be used to control the nanotube packing density, and we vary the shear rate by changing both the channel height and the ink flow rate. We fabricate FETs (channel length 1 – 5 μm) with alignment of ±40°, both parallel and perpendicular to the direction of alignment. The parallel transistors perform with 7× faster mobility (101 and 49 $cm^2V^{-1}s^{-1}$ assuming array and parallel plate capacitances, respectively) with high on/off ratio of 10^5. The mobilities of our FETs exceeds or compares favorably to that of other aligned carbon nanotube FETs fabricated via post-synthetic assembly with on/off ratios greater than 10^3. In addition, however, we also demonstrate uniform deposition of aligned carbon nanotubes across an 8 × 8 cm^2 region. The degree of misalignment present in these films makes this confined shear alignment ideal for long-channel thin film transistors where some misalignment is needed to ensure percolation. Furthermore, the reduction of resistive nanotube/nanotube junctions in these films

indicates confined shear aligned carbon nanotube films will be electrically superior to random nanotube networks currently produced via spin-, dip-, or blade-coating. Finally, optimized conditions enable alignment within a ±32° window, at an intermediate packing density of 50 nanotubes μm^{-1}, on a 10 × 10 cm^2 substrate.

Besides further increasing shear rate, one way to additionally improve alignment within the carbon nanotube films should be to increase the length of the nanotubes in the ink. Increasing length will decrease rotational diffusion coefficient, shifting the curve shown in Figure 2b to the left, thereby yielding better alignment at any given shear rate.

The simplicity of the confined shear alignment apparatus and technique demonstrates that further scaling to even larger areas should be possible and easily implemented. As the technique is further scaled, maintaining uniformity over increasingly larger areas will be aided by the relative insensitivity of both the packing density and the degree of alignment to the deposition conditions (i.e., the packing density is only weakly affected by the number of nanotubes that flow over the substrate once a density of 30 nanotubes μm^{-1} is reached and the degree of alignment is relatively invariant once the shear rate exceeds 1000 s^{-1}). This work is important because, compared to random networks, films of aligned nanotubes promise to be a superior platform for applications including environmental and biological sensors, flexible/stretchable electronics for hybrid, soft, and integrated electronics, and novel light emitting and harvesting devices.

4. Experimental

Preparation of Poly[(9,9-dioctylfluorenyl-2,7-diyl)-alt-co-(6,6'-{2,2'-bipyridine})]-Wrapped Nanotubes. Semiconducting carbon nanotubes are extracted from arc-discharge nanotube soot (Sigma-Aldrich, #698695) using a 1:1 ratio by mass of the raw soot and a polyfluorene derivative polymer wrapper, poly[(9,9-dioctylfluorenyl-2,7-diyl)-*alt-co*-(6,6'-{2,2'-bipyridine})] (PFO-BPy) (American Dye Source, Inc., Quebec, Canada; #ADS153-UV). This soot/PFO-BPy mixture is dispersed at 2 mg mL^{-1} in 60 mL of toluene and sonicated at 40% amplitude with a horn tip sonicator (Fisher Scientific, Waltham, MA; Sonic Dismembrator 500) for 10 min. This solution is centrifuged in a swing bucket rotor (Sorvall WX, TH-641, Thermo-Scientific) at 3×10^5 g for 10 min to remove soot and undispersed nanotubes. The upper 90% of the supernatant is collected and concentrated to a volume of 60 mL. This concentrated supernatant is centrifuged for 18 – 24 h and dispersed in toluene via sonication utilizing the horn tip sonicator. This process of centrifugation and sonication in toluene is repeated three times to remove most of the excess PFO-BPy. The final solution is prepared by horn tip sonication of the rinsed carbon nanotube pellet in chloroform (stabilized with ethanol from Fisher Scientific, #C606SK-1). The concentration of the nanotubes in solution is determined using known optical cross sections from the S_{22} transition.[53]

Preparation of Substrates. Si/SiO_2 substrates with 90 nm or 15 nm of dry, thermal oxide are used in this work. The substrates are cleaned with a piranha solution 2:1 ratio by volume of H_2SO_4 (91 – 92.5%):H_2O_2 (30%) in a crystallizing dish on a 110 °C hot plate for 60 min (for 90 nm oxide) or 15 min (for 15 nm oxide), rinsed with deionized water, and dried with N_2.

Fabrication of Semiconducting Carbon Nanotube FETs. Isolated regions of nanotubes are first defined using electron-beam lithography with polymethylmethacrylate (PMMA) as the resist followed by

development in 2:1 methyl isobutyl ketone (MIBK):IPA for 1 min. Next, an oxygen reactive ion etch is used to remove the exposed nanotubes, and the remaining PMMA is removed with acetone. These patterned nanotube films are boiled in toluene at 120 °C for 1 h and vacuum annealed at 400 °C for 1 h at ~ 10^{-5} torr. Source and drain contacts are then patterned to define the nanotube FET channels via electron-beam lithography using PMMA and the same development described above. Thermal evaporation is used to deposit the contacts, 17.5 nm Pd/17.5 nm Au, the Si substrate is used as a back gate, and 15 nm of SiO_2 is used as the gate dielectric. All devices are measured at room temperature in ambient conditions using a Keithley 2636A SourceMeter.

Spectroscopy Characterization. Raman Spectroscopy (Thermo-Fisher Scientific DXRxi Raman Imaging Microscope) with laser excitation wavelength of 532 nm is used to measure the ratio of the area of the nanotube G-band (~1590 cm^{-1}) to the area of the Si peak (~520 cm^{-1}) to quantify the amount of nanotubes deposited.[61] This G/Si ratio is converted to a linear packing density using a relationship empirically measured from SEM at lower packing densities (shown in **Figure S3**). Prior to Raman measurement, each nanotube film is boiled in toluene at 120 °C for 1 h to remove excess PFO-BPy and then vacuum annealed at 400°C for 1 h at ~ 10^{-5} torr. To ensure there is no effect from any remaining conjugated polymer wrapper on the G-band and G/Si measurement, a control sample is fabricated by performing the confined shear alignment process with a solution of PFO-BPy in chloroform (10 μg mL^{-1}). This control substrate undergoes the post-treatment toluene boil and vacuum anneal as previously stated for the nanotube films. The Raman spectrum from this PFO-BPy control is shown in **Figure S4** and shows no G-band signal. This Raman spectrometer is also employed for the large-area mapping of a confined shear aligned film (Figure 5). Because of the size of the substrate, the sample in Figure 5 cannot be vacuum annealed. Polarized Raman spectroscopy

(Aramis Horiba Jobin Yvon Confocal Raman Microscope) is performed with a laser excitation wavelength of 532 nm by placing linear polarizing filters on both the analyzer and laser.

Supporting Information

Supporting Information is available from the Wiley Online Library.

Acknowledgements

This work was primarily supported by the National Science Foundation (NSF) via SNM-IS award No. 1727523 (K.R.J., J.C., A.B., M.S.A.). K.R.J. furthermore acknowledges support from the NSF Graduate Research Fellowship Program, award No. DGE-1256259. R.M.J. acknowledges support from the U.S. Department of Energy, Office of Science, Basic Energy Sciences, under Award No. DE-SC0016007, for surface-characterization of the shear-alignment apparatus. The authors gratefully acknowledge use of facilities and instrumentation supported by NSF through the University of Wisconsin Materials Research Science and Engineering Center (DMR-1720415). K.R.J. also acknowledges J. Dwyer and M. Shea for helpful discussions on data analysis.

Received: ((will be filled in by the editorial staff))
Revised: ((will be filled in by the editorial staff))
Published online: ((will be filled in by the editorial staff))

References

[1] T. Dürkop, S. A. Getty, E. Cobas, M. S. Fuhrer, *Nano Lett.* **2004**, *4*, 35.

[2] C.-S. Lee, E. Pop, A. D. Franklin, W. Haensch, H.-S. P. Wong, *IEEE Trans. Electron Devices* **2015**, *62*, 3061.

[3] A. D. Franklin, M. Luisier, S.-J. Han, G. Tulevski, C. M. Breslin, L. Gignac, M. S. Lundstrom, W. Haensch, *Nano Lett.* **2012**, *12*, 758.

[4] P. Avouris, J. Appenzeller, R. Martel, S. J. Wind, *Proc. IEEE* **2003**, *9*, 1772.

[5] J.-P. Salvetat, J.-M. Bonard, N. H. Thomson, A. J. Kulik, L. Forro, W. Benoit, L. Zuppiroli, *Appl. Phys. A* **1999**, *69*, 255.

[6] G. S. Tulevski, A. D. Franklin, D. Frank, J. M. Lobez, Q. Cao, H. Park, A. Afzali, S.-J. Han, J. B. Hannon, W. Haensch, *ACS Nano* **2014**, *8*, 8730.

[7] C. Rutherglen, D. Jain, P. Burke, *Nat. Nanotechnol.* **2009**, *4*, 811.

[8] L. Hu, D. S. Hecht, G. Grüner, *Nano Lett.* **2004**, *4*, 2513.

[9] P. N. Nirmalraj, P. E. Lyons, S. De, J. N. Coleman, J. J. Boland, *Nano Lett.* **2009**, *9*, 3890.

[10] G. J. Brady, K. R. Jinkins, M. S. Arnold, *J. Appl. Phys.* **2017**, *122*, 124506.

[11] F. Léonard, *Nanotechnology* **2006**, *17*, 2381.

[12] V. Perebeinos, J. Tersoff, *Phys. Rev. Lett.* **2015**, *114*, 085501.

[13] I. V. Zaporotskova, N. P. Boroznina, Y. N. Parkhomenko, L. V. Kozhitov, *Mod. Electron. Mater.* **2016**, *2*, 95.

[14] J. W. Jo, J. W. Jung, J. U. Lee, W. H. Jo, *ACS Nano* **2010**, *4*, 5382.

[15] V. Derenskyi, W. Gomulya, J. M. S. Rios, M. Fritsch, N. Fröhlich, S. Jung, S. Allard, S. Z. Bisri, P. Gordiichuk, A. Herrmann, U. Scherf, M. A. Loi, *Adv. Mater.* **2014**, *26*, 5969.

[16] Y. Miyata, K. Shiozawa, Y. Asada, Y. Ohno, R. Kitaura, T. Mizutani, H. Shinohara, *Nano Res.* **2011**, *4*, 963.

[17] A. D. Willey, J. M. Holt, B. A. Larsen, J. L. Blackburn, S. Liddiard, J. Abbott, M. Coffin, R. R. Vanfleet, R. C. Davis, *J. Vac. Sci. Technol. B Nanotechnol. Microelectron. Mater. Process. Meas. Phenom.* **2014**, *32*, 011218.

[18] R. C. Tenent, T. M. Barnes, J. D. Bergeson, A. J. Ferguson, B. To, L. M. Gedvilas, M. J. Heben, J. L. Blackburn, *Adv. Mater.* **2009**, *21*, 3210.

[19] V. K. Sangwan, A. Behnam, V. W. Ballarotto, M. S. Fuhrer, A. Ural, E. D. Williams, *Appl. Phys. Lett.* **2010**, *97*, 043111.

[20] M. L. Geier, J. J. McMorrow, W. Xu, J. Zhu, C. H. Kim, T. J. Marks, M. C. Hersam, *Nat. Nanotechnol.* **2015**, *10*, 944.

[21] E. M. Remillard, Q. Zhang, S. Sosina, Z. Branson, T. Dasgupta, C. D. Vecitis, *Carbon* **2016**, *100*, 578.

[22] K. Kordás, T. Mustonen, G. Tóth, J. Vähäkangas, H. Jantunen, A. Gupta, K. V. Rao, R. Vajtai, P. M. Ajayan, *Chem. Mater.* **2007**, *19*, 787.

[23] Abu Bakar Sulong, J. Park, *J. Compos. Mater.* **2011**, *45*, 931.

[24] E. Camponeschi, B. Florkowski, R. Vance, G. Garrett, H. Garmestani, R. Tannenbaum, *Langmuir* **2006**, *22*, 1858.

[25] S. Pujari, W. R. Burghardt, S. S. Rahatekar, A. H. Windle, K. K. Koziol, A. Co, G. L. Leal, R. H. Colby, A. J. Giacomin, in *AIP Conf. Proc.* Vol. 127 (Eds: A. Co, G. L. Leal, R. H. Colby, A. J. Giacomin), Monterery, CA, USA **2008**, 806–808.

[26] X. He, W. Gao, L. Xie, B. Li, Q. Zhang, S. Lei, J. M. Robinson, E. H. Hároz, S. K. Doorn, W. Wang, R. Vajtai, P. M. Ajayan, W. W. Adams, R. H. Hauge, J. Kono, *Nat. Nanotechnol.* **2016**, *11*, 633.

[27] N. Puech, C. Blanc, E. Grelet, C. Zamora-Ledezma, M. Maugey, C. Zakri, E. Anglaret, P. Poulin, *J. Phys. Chem. C* **2011**, *115*, 3272.

[28] B. King, B. Panchapakesan, *Nanotechnology* **2014**, *25*, 175201.

[29] D. D. Tune, B. W. Stolz, M. Pfohl, B. S. Flavel, *Nanoscale* **2016**, *8*, 3232.

[30] Y. Hu, L. Kang, Q. Zhao, H. Zhong, S. Zhang, L. Yang, Z. Wang, J. Lin, Q. Li, Z. Zhang, L. Peng, Z. Liu, J. Zhang, *Nat. Commun. Lond.* **2015**, *6*, 6099.

[31] A. Reina, M. Hofmann, D. Zhu, J. Kong, *J. Phys. Chem. C* **2007**, *111*, 7292.

[32] N. Patil, A. Lin, E. Myers, K. Ryu, A. Badmaev, C. Zhou, H.-S. P. Wong, S. Mitra, *IEEE Trans. Nanotechnol.* **2009**, *8*, 498.

[33] Z. Jin, H. Chu, J. Wang, J. Hong, W. Tan, Y. Li, *Nano Lett.* **2007**, *7*, 2073.

[34] X. Li, L. Zhang, X. Wang, I. Shimoyama, X. Sun, W.-S. Seo, H. Dai, *J. Am. Chem. Soc.* **2007**, *129*, 4890.

[35] V. Sgobba, G. Giancane, D. Cannoletta, A. Operamolla, O. Hassan Omar, G. M. Farinola, D. M. Guldi, L. Valli, *ACS Appl. Mater. Interfaces* **2014**, *6*, 153.

[36] Y. Joo, G. J. Brady, M. S. Arnold, P. Gopalan, *Langmuir* **2014**, *30*, 3460.

[37] G. J. Brady, Y. Joo, M.-Y. Wu, M. J. Shea, P. Gopalan, M. S. Arnold, *ACS Nano* **2014**, *8*, 11614.

[38] K. Jinkins R., J. Chan, G. J. Brady, K. K. Gronski, P. Gopalan, H. T. Evensen, A. Berson, M. S. Arnold, *Langmuir* **2017**, *33*, 13407.

[39] J. Hedberg, L. Dong, J. Jiao, *Appl. Phys. Lett.* **2005**, *86*, 143111.

[40] M. D. Lay, J. P. Novak, E. S. Snow, *Nano Lett.* **2004**, *4*, 603.

[41] P. Kim, T. J. Kang, *Micro Nano Syst. Lett.* **2017**, *5*, 18.

[42] J. Si, D. Zhong, H. Xu, M. Xiao, C. Yu, Z. Zhang, L.-M. Peng, *ACS Nano* **2018**, *12*, 627.

[43] G. J. Brady, A. J. Way, N. S. Safron, H. T. Evensen, P. Gopalan, M. S. Arnold, *Sci. Adv.* **2016**, *2*, e1601240.

[44] Q. Cao, J. Tersoff, D. B. Farmer, Y. Zhu, S.-J. Han, *Science* **2017**, *356*, 1369.

[45] C. Qiu, Z. Zhang, M. Xiao, Y. Yang, D. Zhong, L.-M. Peng, *Science* **2017**, *355*, 271.

[46] Y. Huang, X. Duan, Q. Wei, C. M. Lieber, *Science* **2001**, *291*, 630.

[47] A. Gang, N. Haustein, L. Baraban, W. Weber, T. Mikolajick, J. Thiele, G. Cuniberti, *RSC Adv* **2015**, *5*, 94702.

[48] P. Kim, S. Baik, K. Y. Suh, *Small* **2008**, *4*, 92.

[49] J. Li, Q. Zhang, Y. Yan, S. Li, L. Chen, *IEEE Trans. Nanotechnol.* **2007**, *6*, 481.

[50] G. Yu, A. Cao, C. M. Lieber, *Nat. Nanotechnol.* **2007**, *2*, 372.

[51] R. Zhu, Y. Lai, V. Nguyen, R. Yang, *Nanoscale* **2014**, *6*, 11976.

[52] C. Tannous, *ArXiv09050091 Phys.* **2009**.

[53] K. Mistry, B. Larsen, J. Blackburn, *ACS Nano* **2013**, *7*, 2231.

[54] M. M. Tirado, C. L. Martinez, J. G. de la Torre, *J. Chem. Phys.* **1984**, *81*, 2047.

[55] S. Gerashchenko, V. Steinberg, *Phys. Rev. Lett.* **2006**, *96*, 038304.

[56] A. Celani, A. Puliafito, K. Turitsyn, *Europhys. Lett. EPL* **2005**, *70*, 464.

[57] Y. Joo, G. J. Brady, M. J. Shea, M. B. Oviedo, C. Kanimozhi, S. K. Schmitt, B. M. Wong, M. S. Arnold, P. Gopalan, *ACS Nano* **2015**, *9*, 10203.

[58] Y. Joo, G. J. Brady, C. Kanimozhi, J. Ko, M. J. Shea, M. T. Strand, M. S. Arnold, P. Gopalan, *ACS Appl. Mater. Interfaces* **2017**, *9*, 28859.

[59] M. Engel, J. P. Small, M. Steiner, M. Freitag, A. A. Green, M. C. Hersam, P. Avouris, *ACS Nano* **2008**, *2*, 2445.

[60] Q. Cao, S. Han, G. S. Tulevski, Y. Zhu, D. D. Lu, W. Haensch, *Nat. Nanotechnol.* **2013**, *8*, 180.

[61] T. Maruyama, A. Kozawa, T. Saida, S. Naritsuka, S. Iijima, *Carbon* **2017**, *116*, 128.

Solution-based shear is utilized to align individualized carbon nanotubes at an optimal packing density in continuous films across target substrates. Tailoring the deposition conditions enables alignment of individualized, semiconducting nanotubes within a ±32° window, at 50 nanotubes μm^{-1}, in a continuous film across a 10 × 10 cm^2 substrate. Parallel transistors perform with 7× faster charge carrier mobility.

Wafer-Scale Aligned Carbon Nanotube Films

K. R. Jinkins, J. Chan, R. M. Jacobberger, A. Berson, M. S. Arnold*

Substrate-Wide Confined Shear Alignment of Carbon Nanotubes for Thin Film Transistors